Martínez-Ruiz, D., Huete, C., Sánchez, A. L. & Williams, F. A. (2018). Interaction of Oblique Shocks and Laminar Shear Layers. *AIAA Journal*, 56(3), pp. 1023–1030.

DOI: 10.2514/1.J056302

On the Interaction of Oblique Shocks and Laminar Shear Layers

Daniel Martínez-Ruiz [*], César Huete [†], Antonio L. Sánchez [‡], Forman A. Williams [§]

[*] [†] *Universidad Carlos III de Madrid, Spain.*

[‡] [§] *University of California San Diego, La Jolla, CA 92093-041*

This paper examines the steady interaction of a shear layer separating two uniform supersonic streams of Mach numbers M_1 and M_2 with an oblique shock approaching from the faster stream at an incident angle σ_i sufficiently small for the post-shock flow to remain supersonic everywhere. The development begins by considering the related problem of oblique–shock impingement on a supersonic vortex sheet of infinitesimal thickness, for which the region of existence of regular shock refractions with downstream supersonic flow is delineated in the parametric space (M_1, M_2, σ_i). The interaction region located about the impingement point, scaling with the shear-layer thickness, is described next by integrating the Euler equations in the post-shock region, formulated in characteristic form, subject to the Rankine-Hugoniot jump conditions at the shock front. The results are used to investigate the accuracy and limitations of a simplified treatment, the so-called Moeckel-Chisnell approach, commonly employed for determining the shape of the shock wave in these scenarios, which does not account for the influence of the post-shock flow. It is found that, while the Moeckel-Chisnell method predicts accurately the shape of the shock front as it evolves across the shear layer, it is unable to predict the final transition to the transmitted–shock solution, which occurs beyond the edge of the shear layer. The structure of the shear layer in the far field also is addressed here for the first time, the objective being to lay the groundwork for future studies of shock-induced ignition in supersonic fuel-air mixing layers.

Nomenclature

M	Mach number	T	temperature, nondimensional temperature variation
p	pressure, nondimensional pressure variation	δ	characteristic shear-layer thickness

[*]Lecturer, Fluid Mechanics Group, Universidad Carlos III de Madrid, Spain. dmruiz@ing.uc3m.es

[†]Lecturer, Fluid Mechanics Group, Universidad Carlos III de Madrid, Spain.

[‡]Professor, Department of Mechanical and Aerospace Engineering, University of California San Diego

[§]Professor, Department of Mechanical and Aerospace Engineering, University of California San Diego. AIAA Fellow.

μ	angle of inclination of the two Mach lines with respect to the local flow direction	*Subscript*	
λ	counterclockwise inclination of the streamlines	u	flow properties upstream from the shock
ν	clockwise flow deflection across the shock	s	flow properties right behind the shock
ρ	density	d	farfield flow properties behind the shock
γ	adiabatic index	i	incident
σ	shock angle	t	transmitted
x, z	upstream spatial coordinates	r	reflected
y	downstream transverse coordinate	MC	Moeckel-Chisnell
		PM	Prandtl-Meyer

I. Introduction

The interaction of an oblique shock with a shear layer constitutes a fundamental problem in compressible-flow theory [1]. Such interactions occur, for instance, in combustion chambers of supersonic-combustion ramjets (scramjets), where shocks generated in the air stream at wedged walls and fuel injectors impinge on the shear layer surrounding the fuel jets downstream from the injection point [2]. Although the flow is typically turbulent in these high-Reynolds-number applications, analyses of laminar flows have been shown to be instrumental in providing insightful information pertaining to mixing augmentation by vorticity production [3, 4] and enhanced chemical reaction leading to ignition [5, 6] behind the curved shock.

As in earlier studies, the present work considers a laminar configuration, schematically shown in Fig. 1, involving the interaction of a shear layer of thickness δ_u, separating two supersonic parallel streams with Mach numbers M_1 and $M_2 < M_1$, and an oblique shock with initial incident angle σ_i generated in the faster stream (typically the air stream in scramjet combustors). The front curves as a consequence of the interaction with the nonuniform flow, resulting in a shock inclination $\sigma(z)$ that varies across the shear layer, approaching the value $\sigma = \sigma_t$ for $z \to -\infty$, corresponding to the transmitted shock.

The determination of the shock-front shape poses a complicated free-boundary problem, addressed for the first time by Moeckel [7] for configurations with supersonic flow everywhere in the post-shock region, that also being the case analyzed here. In that case, the influence of the post-shock flow on the shock shape enters in the computation through the Mach lines reaching the shock from behind, identified as the $C-$ characteristics in the figure. An ad-

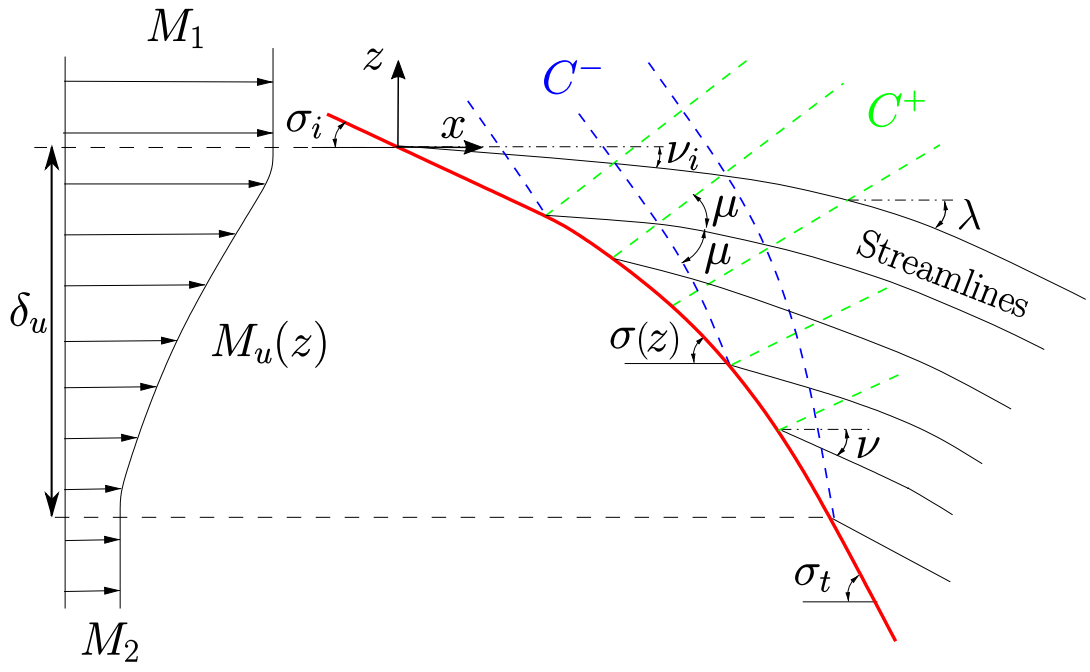

Figure 1. Sketch of the model problem.

hoc simplification was introduced by Moeckel [7] to circumvent this complicating feature of the calculation. His approximate analysis neglects waves "resulting from internal reflection" in the interaction region downstream from the shock, leading to a differential equation that relates the variation of σ with that of the local incident Mach number, so that the Euler-equation problem downstream need not be considered in determining the shock shape.

As noted by Whitham [8], who formulated the method in a more straightforward manner, similar types of approximations were introduced later by Chisnell in independent analyses of shock propagation in tubes of variable area and in nonuniform media [9, 10]. Correspondingly, this approximate computational procedure, adopted for instance in [3, 4], was termed by Whitham [1] the Moeckel-Chisnell approach. Since this approximate theory has no rigorous basis, its applicability must be checked by comparison with exact solutions, as was done previously for the problem of shock propagation in a nonuniform tube [1], for which the accuracy of the results is truly remarkable. The corresponding accuracy quantification has not yet been performed for the problem of shock-wave interaction with a region of nonuniform flow. This is to be accomplished below by comparisons of Moeckel-Chisnell results with numerical solutions of the complete problem.

The structure of the paper is as follows: The combinations of M_1, M_2, and σ_i that lead to supersonic conditions

downstream from the shock are determined in Sec. II by investigation of the related problem of shock-wave refraction at a contact surface. The interaction region is considered next in Sec. III, where the mathematical problem needed to determine the shape of the curved shock front is formulated, with use made of the characteristic form of the conservation equations in the postshock region. Numerical results are compared in Sec. IV with the predictions of the Moeckel-Chisnell theory, including shock-wave shapes and associated temperature distributions, the latter of direct interest in supersonic-combustion applications. Finally, concluding remarks are given in Sec. V.

II. Refraction of an oblique shock at a supersonic vortex sheet

The flow in the interaction region depends on the Mach number distribution across the shear layer upstream from the shock, involving the boundary values M_1 and M_2, and on the inclination angle of the incident shock σ_i. To determine the parametric region (M_1, M_2, σ_i) where the resulting solution corresponds to that envisioned in Fig. 1, it is convenient to begin the analysis by considering the outer flow structure surrounding the interaction region, corresponding to distances from the impingement point much larger than the shear-layer thickness δ_u. At these large distances the shear layer appears infinitesimally thin, so that the problem reduces to that of the interaction of an oblique shock with a contact surface separating two supersonic streams. This seemingly simple problem admits in general multiple solutions depending on the values of M_1, M_2, and σ_i. As discussed in [11], the simplest solutions are regular refractions involving a transmitted shock propagating from the impingement point into stream 2 and a reflected wave propagating into stream 1, thereby defining a total of five regions of uniform flow, as shown in the schematic plots of Fig. 2. The reflected wave can be either a rarefaction or a shock, both having been observed experimentally. These two types of regular expansions can occur only in certain ranges of the controlling parameters, outside of which more complicated irregular-refraction patterns may arise. Theoretical considerations indicate that the "atlas" of possible solutions may include in principle single and double Mach reflections, 4-wave confluences, and continuous expansion bands [12], although only some of these solutions have been observed in experiments. The present considerations are restricted to the cases illustrated in Fig. 2.

For regular refractions, the solution corresponding to given values of M_1, M_2, and σ_i can be determined by application of the jump conditions across the different waves, together with the compatibility conditions across the deflected contact surface. The Rankine-Hugoniot expressions for the pressure jump

$$\frac{p_s}{p_u} = F_p(M_u, \sigma) = \frac{2\gamma M_u^2 \sin^2\sigma + 1 - \gamma}{\gamma + 1}, \tag{1}$$

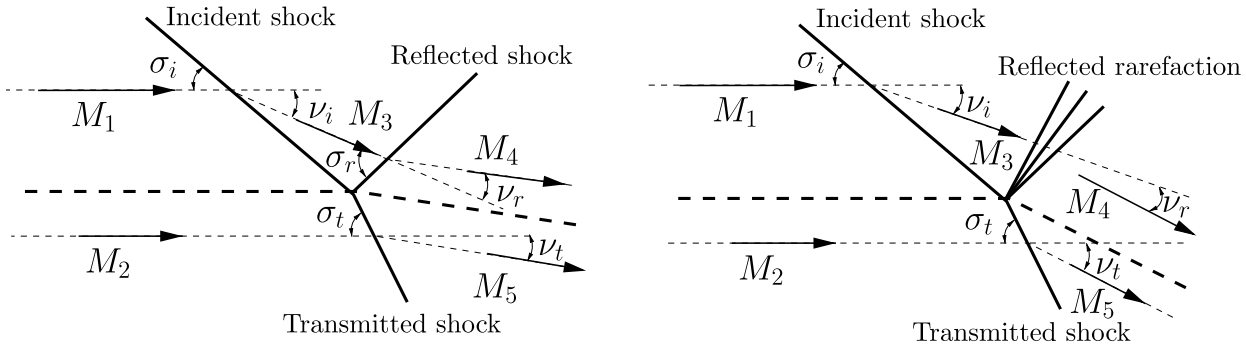

Figure 2. Regular refractions at a supersonic vortex sheet.

flow deflection

$$\nu = F_\nu(M_u, \sigma) = \tan^{-1}\left\{\frac{2(M_u^2 \sin^2\sigma - 1)\cot\sigma}{2 + M_u^2[\gamma + \cos(2\sigma)]}\right\}, \tag{2}$$

and post-shock Mach number

$$M_s^2 = F_M(M_u, \sigma) = \frac{(\gamma+1)^2 M_u^4 \sin^2\sigma - 4(M_u^2\sin^2\sigma - 1)(\gamma M_u^2 \sin^2\sigma + 1)}{(2\gamma M_u^2 \sin^2\sigma + 1 - \gamma)[(\gamma-1)M_u^2 \sin^2\sigma + 2]}, \tag{3}$$

are to be used for the shock waves, with the subscript u and s denoting flow properties immediately upstream and immediately downstream from the shock, respectively. For instance, direct evaluation of these expressions for given values of M_1 and σ_i provides

$$\nu_i = F_\nu(M_1, \sigma_i), \quad p_3/p_u = F_p(M_1, \sigma_i), \quad \text{and} \quad M_3^2 = F_M(M_1, \sigma_i), \tag{4}$$

across the incident shock, where $p_u = p_1 = p_2$ is the pressure of the incoming streams, equal on both sides of the contact surface. On the other hand, across the transmitted shock

$$\nu_t = F_\nu(M_2, \sigma_t), \quad p_5/p_u = F_p(M_2, \sigma_t), \quad \text{and} \quad M_5^2 = F_M(M_2, \sigma_t), \tag{5}$$

for the downstream flow properties below the contact surface, involving the unknown value of the inclination angle σ_t.

When the reflected wave is a shock, the case shown in the first plot of Fig. 2, the expressions

$$\nu_r = F_\nu(M_3, \sigma_r), \quad p_4/p_3 = F_p(M_3, \sigma_r), \quad \text{and} \quad M_4^2 = F_M(M_3, \sigma_r) \tag{6}$$

apply to the downstream flow properties above the contact surface. Correspondingly, equations (4), (5), and (6) together with the two additional contact-surface conditions

$$(p_4/p_3)(p_3/p_u) = (p_5/p_u) \quad \text{and} \quad \nu_t = \nu_i - \nu_r \tag{7}$$

provide a set of eleven algebraic equations that determine M_3, M_4, M_5, σ_r, σ_t, ν_i, ν_r, ν_t, p_3/p_u, p_4/p_u, and p_5/p_u as a function of M_1, M_2, and σ_i for a regular refraction with a reflected shock wave. When the reflected wave is an expansion, however, the expressions (6) must be replaced, with $\sigma_r = \sin^{-1}(M_3)$, by

$$\left(\frac{p_4}{p_3}\right)^{\frac{\gamma-1}{\gamma}} = \frac{1+\frac{\gamma-1}{2}M_3^2}{1+\frac{\gamma-1}{2}M_4^2}, \quad \text{and} \quad \nu_r = F_{\rm PM}(M_4) - F_{\rm PM}(M_3), \tag{8}$$

where

$$F_{\rm PM}(M) = \left(\frac{\gamma+1}{\gamma-1}\right)^{1/2} \tan^{-1}\left\{\left[\frac{\gamma-1}{\gamma+1}(M^2-1)\right]^{1/2}\right\} - \tan^{-1}\left[(M^2-1)^{1/2}\right], \tag{9}$$

is the Prandtl-Meyer function. In that case, the computation involves (4), (5), (7), and (8), with $-\nu_r$ replaced by $+\nu_r$ in the second equation of (7), as corresponds to the clockwise deflection associated with the reflected rarefaction.

The interaction region depicted in Fig. 1 is located in the vicinity of the impingement point where the incident, transmitted, and reflected waves meet. The streamlines in the shear layer curve as they cross the downstream interaction region. Far downstream all streamlines are parallel again, with deflection ν_t corresponding to that indicated in Fig. 2 behind the reflected and transmitted shocks. Correspondingly, the values of the Mach number behind the reflected wave M_4 and behind the transmitted wave M_5 correspond to the values of the downstream Mach number for the two streamlines bounding the shear layer from above and from below, respectively. In general, the separation between these two boundary streamlines differs from the initial separation δ_u, as is needed to satisfy continuity.

Attention is given here to configurations for which the flow downstream from the curved shock remains supersonic, corresponding to regular refractions satisfying both $M_4 > 1$ and $M_5 > 1$, the second condition being more restrictive for shear layers with $M_1 > M_2$. The range of values of M_1, M_2, and σ_i for which such regular refractions exist was investigated by use of the above algebraic equations. To that end, for given fixed values of M_1 and σ_i satisfying $M_1 \sin\sigma_i \geq 1$ and $M_3 \geq 1$, the value of M_2 was progressively reduced from $M_2 = M_1$ until a value of M_2 was achieved at which $M_5 = 1$.

The resulting value of M_2 is represented by isocurves on the $M_1 - \sigma_i$ plane of Fig. 3 for $\gamma = 1.4$. The upper and lower boundaries in the plot are defined by the conditions $M_3 = 1$ and $M_1 \sin\sigma_i = 1$. For the case $M_2 < M_1$ considered here, it is found that under most conditions the refraction involves a reflected rarefaction, while reflected shocks occur only in a small parametric region located near the upper left corner of Fig. 3, corresponding to low-velocity streams and relatively large incident angles. The subsequent analyses therefore pertain to the other region, corresponding to the second plot in Fig. 2, encompassing the cases of greatest interest.

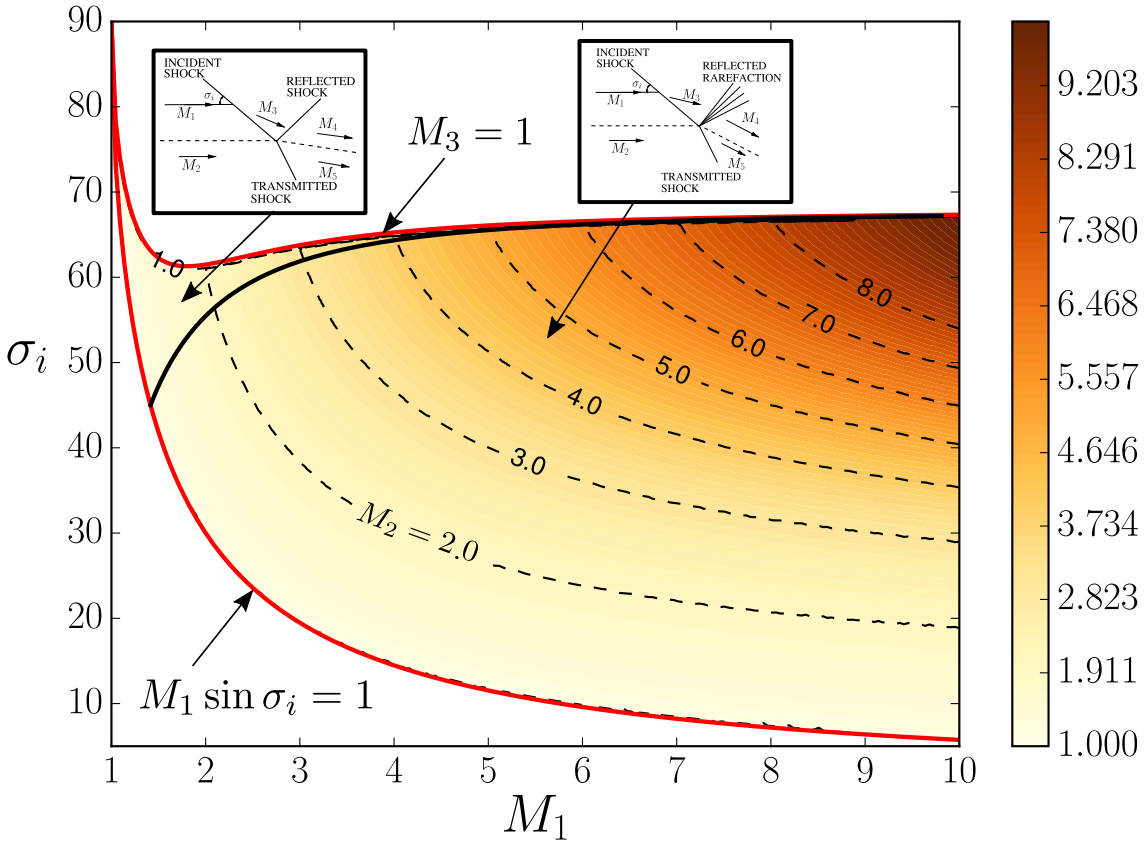

Figure 3. The value of M_2 for $M_5 = 1$ when $\gamma = 1.4$.

For a given value of M_2, the corresponding dashed isocontour in Fig. 3 defines the upper boundary of the parametric region $M_1 - \sigma_i$ where regular refractions with supersonic flow can be encountered, in that for higher values of σ_i the corresponding solution, if it exists al all, would involve values of $M_5 < 1$. The additional condition $M_1 > M_2$ provides an additional boundary for the parametric region of interest, which is depicted in the plots of Fig. 4 for the particular case $M_2 = 4$. Isocurves are employed to represent the values of the post-shock Mach number of the transmitted shock M_5 (first plot) and its inclination σ_t, obtained from the solution to the set of eleven algebraic equations.

III. Formulation of the shock-wave/shear-layer interaction problem

The description of the interaction region employes the shear-layer thickness δ_u to define dimensionless cartesian coordinates (x, z), centered at the point where the shock impinges on the upper edge of the shear layer, with x aligned with the approaching flow and z pointing towards the faster stream, as indicated in Fig. 1. Correspondingly, the shape

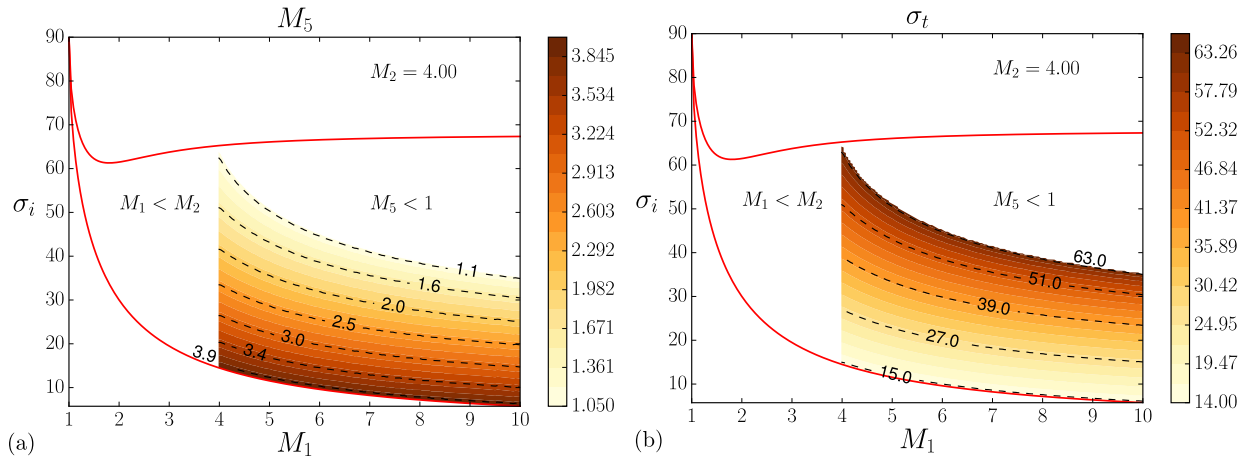

Figure 4. Parametric region where a regular refraction with supersonic post-shock flow may occur when $M_2 = 4$, with isocurves used to indicate the resulting Mach number behind the transmitted shock (a) and the inclination of the transmitted shock (b).

of the shock front $x = x_s(z)$ is given by

$$x_s = -\int_0^z \frac{\mathrm{d}z}{\tan\sigma(z)} \tag{10}$$

in terms of the shock inclination $\sigma(z)$, which in turn depends on the Mach-number distribution upstream from the shock $M_u(z)$.

As previously indicated, the computation of $\sigma(z)$ for a given $M_u(z)$ constitutes a complicated free-boundary problem involving the integration of the Euler equations downstream from the shock, with the conditions immediately behind the shock determined by application of the Rankine-Hugoniot relations given in (1)–(3). The previous shock-refraction analysis has served to identify the values of M_1, M_2, and σ_i for which the flow behind the curved front remains everywhere supersonic (e.g. values of M_1 and σ_i within the shaded region of Fig. 4 would provide such conditions when $M_2 = 4$). For supersonic flow the Euler equations can be formulated in characteristic form, with three different characteristic lines crossing any given point. The entropy is conserved along the streamlines in the post-shock region, a condition that can be expressed in the form

$$\frac{\mathrm{d}p}{p} - \frac{\gamma}{2}\frac{\mathrm{d}(M^2)}{1+\frac{\gamma-1}{2}M^2} = 0, \quad \text{on} \quad \frac{\mathrm{d}z}{\mathrm{d}x} = \tan\lambda, \tag{11}$$

where p is the pressure, M is the Mach number, and λ is the (counterclockwise) local angle of deflection of the streamlines with respect to the horizontal. On the other hand, manipulation of the conservation equations for continuity and momentum provides the two additional characteristic equations [13]

$$\frac{\mathrm{d}p}{p} \pm \frac{\gamma M^2}{\sqrt{M^2-1}}\mathrm{d}\lambda = 0, \quad \text{on} \quad \frac{\mathrm{d}z}{\mathrm{d}x} = \tan(\lambda \pm \mu), \tag{12}$$

where $\mu = \sin^{-1}(1/M)$ defines the angle of inclination of the two Mach lines relative to the local flow direction, as depicted in Fig. 1.

The integration along the streamlines and along the C^+ characteristic lines $\mathrm{d}z/\mathrm{d}x = \tan(\lambda + \mu)$ starts at the shock, with corresponding initial conditions

$$p/p_u = F_p[M_u(z), \sigma], \quad \lambda = -\nu = -F_\nu[M_u(z), \sigma], \quad M^2 = F_M[M_u(z), \sigma], \quad \text{at} \quad x = x_s(z), \tag{13}$$

involving the Rankine-Hugoniot functions defined in (1)–(3). On the other hand, the C^- characteristics originate in the shocked stream above the shear layer, so that the associated uniform properties of region 3 must be used as initial conditions, to be imposed along the C^+ characteristic line leaving the impingement point according to

$$p/p_u = p_3/p_u, \quad \lambda = -\nu_3, \quad M = M_3, \quad \text{at} \quad x = \frac{z}{\tan[\sin^{-1}(1/M_3) - \nu_i]}. \tag{14}$$

The integration must be continued until the C^- characteristic line intersects the shock, providing the information needed at each point to determine the shock curvature $\mathrm{d}\sigma/\mathrm{d}z$.

To the best of our knowledge, the problem formulated above has never been solved. Previous computations (see e.g. [3, 4]) incorporate instead the approximate Moeckel-Chisnell analytic method for determining the shock shape $\sigma(z)$. As explained by Whitham [1], the Moeckel-Chisnell approach amounts to applying the relation

$$\frac{\mathrm{d}p}{p} = \frac{\gamma M^2 \mathrm{d}\lambda}{\sqrt{M^2 - 1}}, \tag{15}$$

corresponding to the C^- characteristic line of (12), along the shock front. Differentiating the first two equations in (13) and substituting the result into the above equation yield

$$\frac{\mathrm{d}\sigma}{\mathrm{d}M_u} = -\frac{A_p + \gamma F_M A_\nu/(F_M - 1)^{1/2}}{B_p + \gamma F_M B_\nu/(F_M - 1)^{1/2}} \tag{16}$$

as a local expression for the shock evolution, where the functions F_M,

$$A_p = \frac{1}{F_p}\frac{\partial F_p}{\partial M}, \quad B_p = \frac{1}{F_p}\frac{\partial F_p}{\partial \sigma}, \quad A_\nu = \frac{\partial F_\nu}{\partial M}, \quad \text{and} \quad B_\nu = \frac{\partial F_\nu}{\partial \sigma} \tag{17}$$

can be evaluated explicitly in terms of σ and M_u with use made of the definitions given in (1)–(3). In the Moeckel-Chisnell approach, integration of (16) with initial condition $\sigma = \sigma_i$ at $M_u = M_1$ provides $\sigma = \sigma_{\mathrm{MC}}(M_1, \sigma_i, M_u)$, which increases with decreasing M_u. One can use this function to determine the shock inclination $\sigma(z)$ for a given upstream Mach-number distribution $M_u(z)$, with the front shape $x_s(z)$ following by straightforward integration of (10).

IV. Comparisons of the numerical results with the Moeckel-Chisnell predictions

IV.A. Representative numerical results

To generate specific numerical results a choice must be made for the upstream Mach-number distribution $M_u(z)$ of Fig. 1. Sample results are discussed here corresponding to the representative selection

$$\begin{cases} M = M_1 & \text{for } z > 0 \\ M = \frac{1}{2}(M_1 + M_2) + \frac{1}{2}(M_1 - M_2)\sin\left[\pi(z + \frac{1}{2})\right] & \text{for } 0 > z > -1 \\ M = M_2 & \text{for } -1 > z \end{cases} \tag{18}$$

as shown in Fig. 5 for $M_1 = 10$, $M_2 = 4$, and $\sigma_i = 30^\circ$. Besides maps of the flow inclination λ, the dimensionless pressure p/p_u, and the Mach number M, a plot is included for the distribution of temperature, computed by considering the conservation of stagnation temperature along streamlines, with a uniform temperature T_u assumed upstream from the shock.

The computations reveal that the variation of $\sigma(z)$ is non-monotonic, resulting in a curved shock front with an inflection point at the lower boundary of the shear layer, corresponding to a local maximum of the incident angle, indicated by a dot in Fig. 5. The non-negligible shock deflection occurring below the inflection point, in the region where the upstream Mach-number profile is already uniform, is a consequence of the interactions of the C^- characteristics with the shock, resulting in a decrease of the incident angle. The value of σ eventually approaches the value σ_t corresponding to the inclination of the transmitted wave $\sigma_t \simeq 51^\circ$.

IV.B. Moeckel-Chisnell shock-wave shapes

The plots of Fig. 5 include also the shape of the shock front predicted with the Moeckel-Chisnell theory, obtained by integration of (16) with initial condition $M_1 = 10$ and $\sigma_i = 30^\circ$, followed by use of (10) supplemented with (18). The differences between the predicted shape and the numerical results are almost invisible throughout the shear layer, but they become somewhat more noticeable farther below, as the shock front curves to approach the inclination angle σ_t, while the approximation remains a straight line after exiting the shear layer very near the inflection point of the numerical results. The Moeckel-Chisnell theory thus fails to predict the inflection.

These differences are investigated further in Fig. 6. According to (16), the inclination of the shock predicted by the Moeckel-Chisnell method reaches its maximum value $\sigma_{\rm MC}(M_1, \sigma_i, M_2)$ at the lower edge of the shear layer, and remains constant farther below, in the region of uniform flow where M_u is constant, as indicated above. The

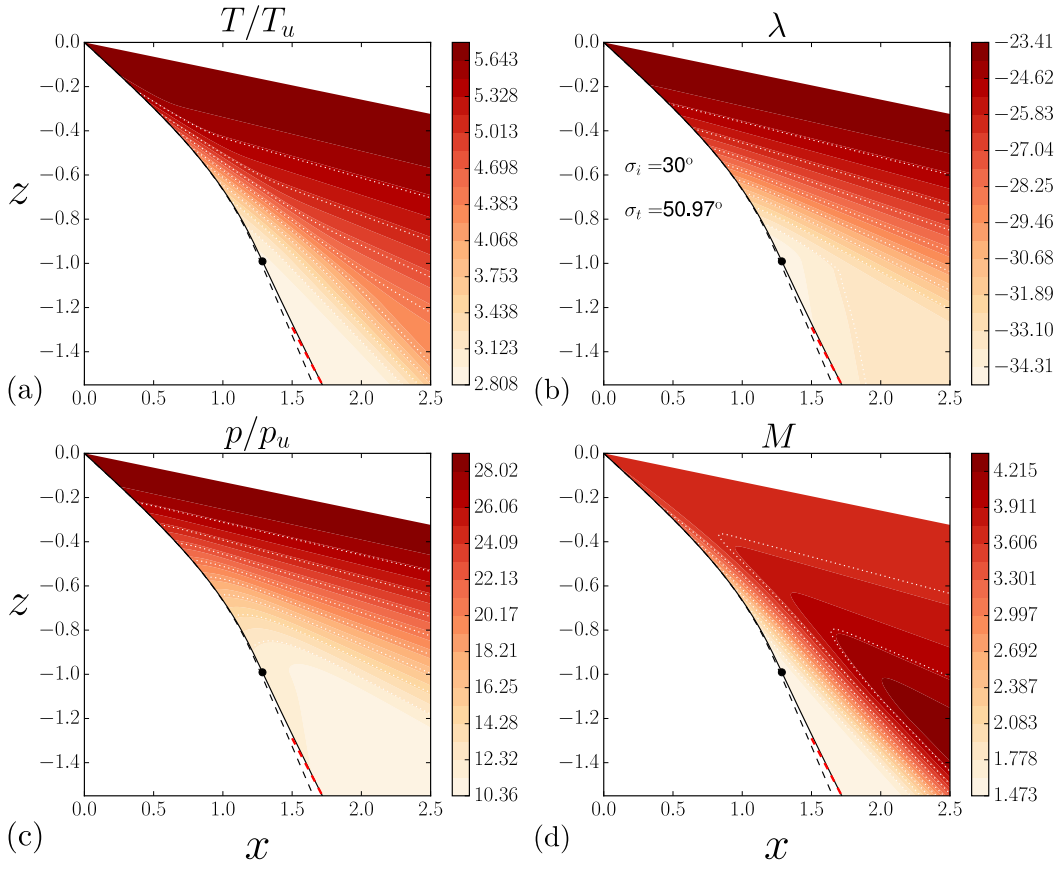

Figure 5. Results corresponding to $M_1 = 10$, $M_2 = 4$, and $\sigma_i = 30^o$ including distributions of temperature (a), deflection angle (b), pressure (c), and Mach number (d) for $\gamma = 1.4$; the inflection point of the shock front is indicated with an enlarged dot. The dashed curves without an inflection represent the Moeckel-Chisnell prediction corresponding to these conditions while the solid line indicates the inclination σ_t of the transmitted shock as obtained from the numerical integration.

resulting value of $\sigma_{\rm MC}(M_1, \sigma_i, M_2)$ is always larger than the inclination of the transmitted wave by an amount that depends on the specific conditions considered. This difference $\sigma_{\rm MC}(M_1, \sigma_i, M_2) - \sigma_t$, which is plotted in Fig. 6 for $M_2 = 4$, becomes greater for larger values of M_1 and σ_i, with the largest differences found for conditions such that M_5 approaches unity (i.e. near the upper boundary of the accessible region in the $M_1 - \sigma_i$ plane). For example, for $M_1 = 10$ and $\sigma_i = 30^o$ we find $\sigma_{\rm MC}(M_1, \sigma_i, M_2) - \sigma_t \simeq 12^o$, corresponding to the shock of Fig. 5.

IV.C. Predictions of post-shock properties

For a given shock inclination $\sigma(z)$, associated with a Mach number distribution $M_u(z)$, the Rankine-Hugoniot jump conditions provide the distribution of flow properties immediately behind the shock, identified by the subscript s

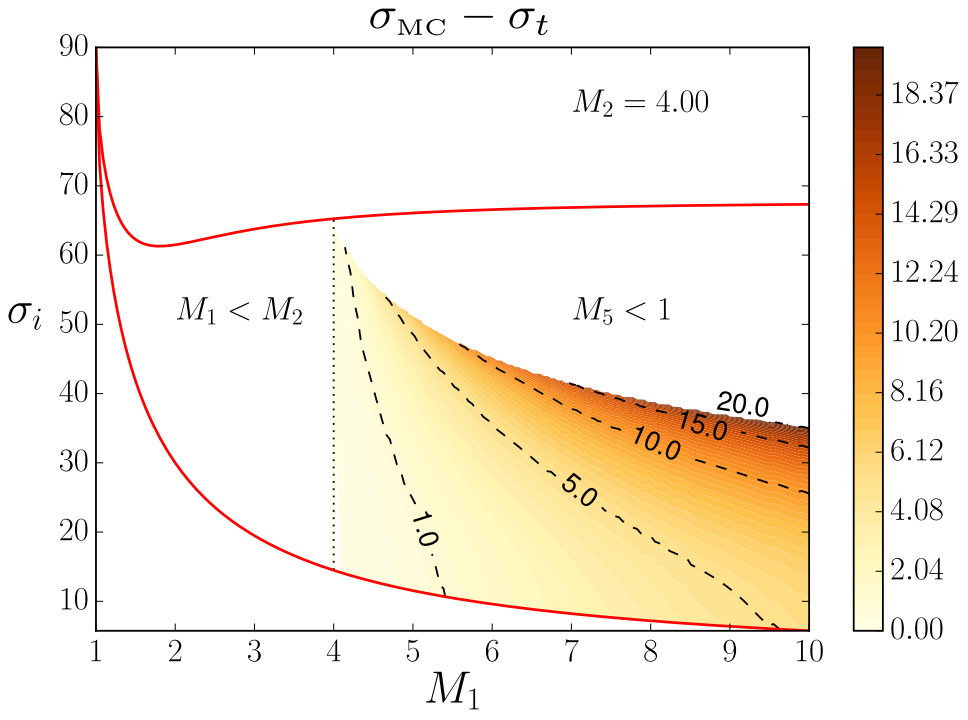

Figure 6. The difference between the inclination of the transmitted shock, σ_t, and that predicted by Moeckel-Chisnell method at the lower edge of the shear layer, $\sigma_{\rm MC}(M_1, \sigma_i, M_2)$, for $M_2 = 4$ when $\gamma = 1.4$.

in the following discussion. For instance, the post-shock Mach number $M_s(z)$ and the stagnation pressure $(1 + \frac{\gamma-1}{2}M_s^2)^{\gamma/(\gamma-1)}(p_s/p_u)$ can be obtained from

$$M_s^2(z) = F_M(M_u, \sigma) \quad \text{and} \quad \left(1 + \frac{\gamma-1}{2}M_s^2\right)^{\gamma/(\gamma-1)}(p_s/p_u) = \left[1 + \frac{\gamma-1}{2}F_M(M_u, \sigma)\right]^{\gamma/(\gamma-1)} F_p(M_u, \sigma), \tag{19}$$

where F_p and F_M are defined in (1) and (3), respectively. Post-shock profiles evaluated with the shock-inclination $\sigma(z)$ determined by numerical integration of (11)–(14) for the Mach-number distribution (18) with $M_1 = 10$ and $M_2 = 4$ are plotted in Fig. 7 for three different values of the incident–shock angle $\sigma_i = (20°, 25°, 30°)$. The results are compared with the corresponding Moeckel-Chisnell predictions, obtained with use made of the function $\sigma_{\rm MC}(M_1, \sigma_i, M_u)$ as calculated from (16), in evaluating the functions F_p and F_M in (19). As expected from the agreement in shock-front shapes observed in Fig. 5, the approximate Moeckel-Chisnell theory gives very accurate post-shock distributions for $-1 \le z \le 0$. Significant departures are noticeable only below the lower edge of the shear layer, in the region $z < -1$ where the shock inclination decreases to approach σ_t, an effect not captured in the Moeckel-Chisnell approximation.

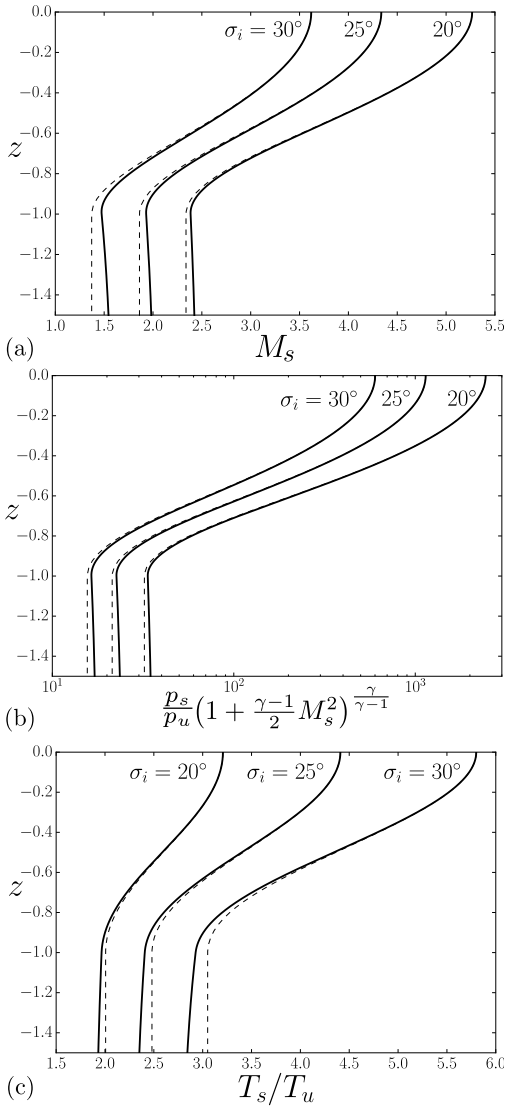

Figure 7. Post-shock distributions of Mach number (a), stagnation pressure (b), and temperature (c) as given by Moeckel-Chisnell approximation (dashed) and numerical integration (solid) for $M_1 = 10$, $M_2 = 4$, and $\sigma_i = 20°, 25°, 30°$, with $\gamma = 1.4$.

The interaction problem investigated here is relevant in particular for supersonic-combustion applications, in which local compression by shock waves impinging on mixing layers separating the air and fuel streams may promote autoignition by raising the temperature of the shocked gas. Post-shock temperature distributions are needed in computing ignition events. As discussed in [5], depending on the conditions, ignition may occur either in a localized ignition kernel adjacent to the shock or at a distant location downstream from the interaction region. For these reasons, there is interest in the computation of temperature distributions both immediately downstream from the shock, T_s, and also across the mixing layer in the far field, T_d. The former can be obtained by using conservation of stagnation temperature

across the shock to yield

$$\frac{T_s}{T_u} = \frac{1 + \frac{\gamma-1}{2} M_u^2}{1 + \frac{\gamma-1}{2} F_M(M_u, \sigma)}. \tag{20}$$

This equation is used in Fig. 7 to evaluate the temperature profiles for the specific conditions of that figure. Besides evaluations obtained with the value of σ corresponding to the numerical integrations of the post-shock Euler problem, the figure represent as dashed curves the temperature profiles evaluated with the function $\sigma_{\rm MC}(M_1, \sigma_i, M_u)$. As occurs with the other post-shock properties discussed above, the predictions of the Moeckel-Chisnell theory are seen to be very accurate across the shear layer, with noticeable differences appearing only near the lower edge and beyond. In non-premixed supersonic-combustion systems ignition can only occur inside the mixing layer separating the fuel and air streams, where both reactants are present, whence the departures observed in Fig.7, which affect mostly the temperature distribution outside the shear layer, are inconsequential for ignition. These results therefore indicate that the computation of critical ignition conditions can make use of the Moeckel-Chisnell theory in evaluating the post-shock temperatures with good accuracy, as was done in earlier analyses [5, 6].

IV.D. The structure of the shear layer in the far field

The temperature across the shear layer continues to evolve downstream from the shock as a result of the interaction with the pressure waves. As the pressure approaches the final value $p_d = p_4 = p_5$, determined by the regular-refraction analysis presented in Sec. II, the temperature and Mach number settle into the final asymptotic distributions $T_d(y)$ and $M_d(y)$, where y is the distance to the upper edge of the mixing layer, scaled with the upstream thickness δ_u. In the computation of these profiles it is convenient to consider the flow along a given streamline, identified by its upstream position z. The final Mach number $M_d(z)$ can be computed by using conservation of stagnation pressure downstream along streamlines from the shock to give

$$M_d(z) = \left(\frac{2}{\gamma-1}\right)^{1/2} \left\{ \left[1 + \frac{\gamma-1}{2} F_M(M_u, \sigma)\right] \left[\frac{p_u}{p_d} F_p(M_u, \sigma)\right]^{\frac{\gamma-1}{\gamma}} - 1 \right\}^{1/2}, \tag{21}$$

whereas the final temperature is related to the upstream distribution by

$$\frac{T_d(z)}{T_u(z)} = \frac{1 + \frac{\gamma-1}{2} M_u^2(z)}{1 + \frac{\gamma-1}{2} M_d^2(z)}, \tag{22}$$

corresponding to conservation of stagnation temperature. The relative downstream position y of the streamline initially located at z follows from the condition of conservation of mass applied to a differential stream tube written in the form

$(p_u M_u/\sqrt{T_u})\mathrm{d}z = (p_d M_d/\sqrt{T_d})\mathrm{d}y$. Integrating from the upper edge of the shear layer yields

$$y = \frac{p_u}{p_d}\int_0^z \frac{M_u(z)}{M_d(z)}\left(\frac{1+\frac{\gamma-1}{2}M_u^2(z)}{1+\frac{\gamma-1}{2}M_d^2(z)}\right)^{1/2}\mathrm{d}z, \tag{23}$$

which, when evaluated at the lower edge of the shear layer, yields

$$\frac{\delta_d}{\delta_u} = \frac{p_u}{p_d}\int_{-1}^0 \frac{M_u(z)}{M_d(z)}\left(\frac{1+\frac{\gamma-1}{2}M_u^2(z)}{1+\frac{\gamma-1}{2}M_d^2(z)}\right)^{1/2}\mathrm{d}z \tag{24}$$

for the final shear-layer thickness δ_d. Equations (21), (22), and (23) determine implicitly the asymptotic profiles $T_d(y)$ and $M_d(y)$.

Figure 8 shows the far-downstream profiles of the temperature ratio and the Mach number for the same conditions as those in Fig. 7. Although these results were computed employing the full numerical simulation for the shock wave in the shear-layer region, differences that would be obtained by employing the Moeckel-Chisnell approximation instead would be very small, as can be inferred from the comparisons in Fig. 7. It may be seen from Fig. 8 that in all cases the range of y over which appreciable variations of the profiles occur is approximately 0.4. This indicates that the final shear-layer thickness δ_d is less than half the initial shear-layer thickness δ_u even though it is clear, for example from Fig. 1, that some streamline divergence occurs as the gas flows downstream from the shock. Temperature decreases of fluid elements will be associated with the streamline divergence, but, since the divergence is small, this temperature decrease will not be large. In applying these results to address shock-induced ignition in supersonic fuel-air mixing layers, therefore, when conditions are such that ignition does not occur right behind the shock, in most instances it will be a reasonable approximation to assume that ignition occurs essentially at far-field gas conditions. In that respect, it may be noted that, in pursuing the mixing-layer analysis, for the effectively inviscid range considered here, the final mass fraction distribution of a chemical species $Y_d(y)$ is given simply by the equation $Y_d(z) = Y_u(z)$, stating the constancy of the composition along any given streamline, given by (22).

V. Concluding Remarks

A principal finding of the present investigation is that, for the entirely supersonic shear layers addressed here, the Moeckel-Chisnell approximation, in which the conditions that apply along the family of characteristics that extends from the stream at the higher Mach number (within which an oblique shock originates) towards the stream of lower Mach number, are applied instead along the curving oblique shock, produces very good accuracy for the shock shape and shock jump conditions throughout the shear layer. The approximation deteriorates increasingly with increasing

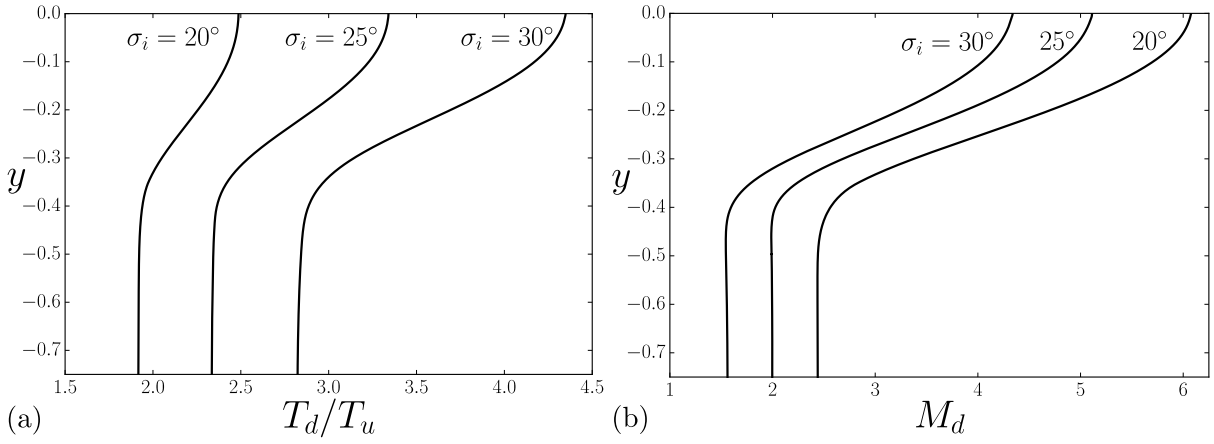

Figure 8. Far-field temperature distribution (a) and Mach-number profiles (b) for $M_1 = 10$, $M_2 = 4$, and $\sigma_i = 20°, 25°, 30°$, with $\gamma = 1.4$.

distance into the stream of lower Mach number, having failed to predict the inflection point in the shape of the oblique shock, required to recover the correct far-field solutions in which the shear layer reduces to a slip surface. The full numerical integration predicting the flow field, accomplished here for the first time, by use of the characteristic coordinates, demonstrates clearly that the inflection point in the oblique-shock profile always is essential in a fully proper description of this flow.

As a preliminary step in addressing oblique-shock-induced initiation of combustion in supersonic fuel-air mixing layers, the present study supports the good accuracy of adoption of the Moeckel-Chisnell approximation to obtain significant simplifications in such analyses. For example, for conditions under which ignition occurs close behind the oblique shock, that approximation results in a very good approximation for the thermodynamic state in the ignition kernel. In less reactive mixtures the ignition will occur farther downstream, and, by including analysis of the far-field flow in the shear layer, the present work provides the thermodynamic conditions needed for pursuing ignition analyses, irrespective of their bases, which may range from one-step-chemistry approximations to descriptions involving detailed chemistry. It has been seen here that the changes in the chemistry-free thermodynamic state along streamlines, from the oblique shock to the far field, are generally small enough that the far-field state usually may be employed with reasonable accuracy in ignition investigations when combustion is not initiated right behind the shock.

Acknowledgments

This work was supported by the US AFOSR Grant No. FA9550-16-1-0443 (A.L.S. and F.A.W.) and by the Ministry of Science, MEC (ENE2015-65852-C2-2-R), Spain (C.H. and D.M-R).

References

[1] Whitham G.B. "Linear and Nonlinear Waves." Wiley, New York, 1974. doi: 10.1002/9781118032954

[2] Laurence S.J., Karl S., Schramm J., Martínez, J., Hannemann, K., "Transient fluid-combustion phenomena in a model scramjet." J. Fluid Mech. Vol. 722, 2013, pp. 85–120. doi: 10.1017/jfm.2013.56

[3] Buttsworth D.R., "Interaction of oblique shock waves and planar mixing regions" J. Fluid Mech. Vol. 306, 1996, pp. 43–57. doi: 10.1017/S002211209600122X

[4] Tritarelli R. C., Kleiser, L., "Vorticity-production mechanisms in shock/mixing-layer interaction problems." Shock Waves, Vol. 27, 2017, pp. 143–52. doi: 10.1007/s00193-016-0636-1

[5] Huete C., Sánchez A.L., Williams F.A., Urzay, J., "Diffusion-flame ignition by shock-wave impingement on a supersonic mixing layer." J. Fluid Mech. Vol. 784, 2015, pp. 74–108. doi: 10.1017/jfm.2015.585

[6] Huete C., Sánchez A.L., Williams F.A., "Diffusion-flame ignition by shock-wave impingement on a hydrogen-air supersonic mixing layer." J. Prop. Power. Vol. 33, 2017, pp. 256–263. doi: 10.2514/1.B36236

[7] Moeckel W.E., "Interaction of oblique shock waves with regions of variable pressure, entropy, and energy". NACA Tech. Note 2725, 1952.

[8] Whitham G.B. "On the propagation of shock waves through regions of non-uniform area or flow." J. Fluid Mech. Vol. 4, 1958, pp. 337–360. doi: 10.1017/S0022112058000495

[9] Chisnell R.F. "The normal motion of a shock wave through a non-uniform one-dimensional medium." Proc. Roy. Soc. Lon. A Vol. 232, 1955, pp. 350–370. doi: 10.1098/rspa.1955.0223

[10] Chisnell R.F. "The motion of a shock wave in a channel, with applications to cylindrical and spherical shock waves." J. Fluid Mech. Vol. 2, 1957, pp. 286–298. doi: 10.1017/S0022112057000130

[11] Landau L.D., Lifshitz E.M. "Fluid Mechanics" Second ed., Pergamon Press, London, UK 1987, p. 423.

[12] Henderson L.F., Macpherson A.K. “On the irregular refraction of plane shock wave at a Mach number interface” J. Fluid Mech. Vol. 32, 1968, pp. 185–202. doi: 10.1017/S0022112068000650

[13] Hayes W.D., Probstein R.F., “Hypersonic Inviscid Flow”, Second ed., Dover, Mineola, NY, 2004.